Scanning mirror microscope with optical sectioning characteristics: applications in ophthalmology

Charles J. Koester

Optical sectioning is the simultaneous illumination and viewing of only a thin region of a specimen. An illuminated slit is imaged at the plane of interest and is swept laterally by the action of an oscillating mirror. The light returning from the specimen reflects from a second facet of the oscillating mirror and forms a stationary image of the illuminated slit. At this stationary image a second slit is placed, which passes light from the desired plane and rejects scattered light from other depths within the specimen. Light passing through the second slit is reflected from the third facet of the oscillating mirror and is focused to the final image plane. The image is reconstructed as the image of the second slit sweeps across the image plane. An important ophthalmological application is the examination of the endothelial cell layer of the cornea, either by contact or noncontact techniques. Optimization for image illuminance and resolution is discussed.

I. Introduction

In a number of biological and medical applications there is a need to examine detail within a semitransparent or scattering medium using incident light microscopy. The problem is to prevent light scattered in regions above and below the plane of interest from contributing stray light to the image.

An example is the corneal endothelial cell layer, a monolayer of cells on the inside surface of the cornea (see Fig. 1). While the entire cornea is normally transparent, it is important to examine the endothelial cells in cases of corneal disease, which is often accompanied by scattering in the central region of the cornea, the stroma. In addition, reflection can occur from the cornea surface (T in Fig. 1), which further increases the possibility of stray light in the image. The endothelial cells themselves are not strongly scattering and are therefore difficult to see. As early as 1920 it was shown by Vogt[1] that endothelial cells could be seen by specular reflection using the narrow beam illumination provided by a biomicroscope (a slit lamp). The specular reflection occurs at the relatively flat interface between the cells and the aqueous, located posterior to the endothelium. An important advance was made by Maurice,[2] who found that the endothelial cells could be viewed at high magnification by illuminating through half of a microscope objective and forming the image using the other half of the objective (Fig. 2). The illuminated area was in the form of a slit, typically 100 by 500 μm. Because of the narrow illuminated region and the oblique incidence, stray light from regions above the endothelium was minimized. This concept was developed to clinically useful instruments by Laing *et al.*[3] and by Bourne and Kaufman.[4,5]

To record a larger field and achieve an optical section, Maurice developed a scanning slit microscope.[6] In this design the specimen was moved past a stationary illuminated slit image, while the film was moved synchronously behind a stationary slit in the image plane. This system gave detailed photomicrographs of the endothelium and of structure within the stroma. However, it did not permit direct viewing of the image, and it was not adaptable to clinical situations.

Another approach to wide field incident light microscopy was patented by Baer.[7] To our knowledge it has not been applied to the problem of endothelial cell visualization.

For the problem of visualizing cellular detail within living tissue, Davidovits and Egger[8] built a scanning laser microscope in which the microscope objective was scanned raster fashion over the specimen. In an earlier paper, Petran *et al.*[9] used a rotating scanning disk (Nipkow wheel) for synchronous scanning of illumination and imaging apertures across the specimen. These

The author is with Columbia University, College of Physicians & Surgeons, Ophthalmology Department, New York, New York 10032.

Received 25 October 1979.
0003-6935/80/111749-09$00.50/0.

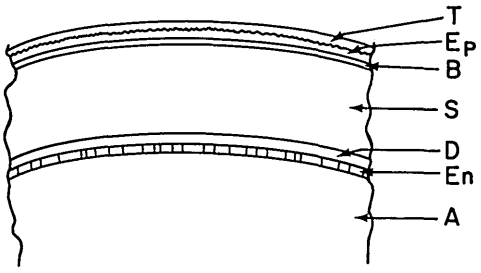

Fig. 1. Cross section of the cornea, not to scale: *T*, tear film; *Ep*, epithelial cell layer; *B*, Bowman's membrane; *S*, stroma; *D*, Descemet's membrane; *En*, endothelial cell layer; *A*, aqueous.

approaches produced optical sections as thin as ~20 μm. Optical quality of the images was limited by the presence of prominent scan lines.

The objective of the present study was to develop a wide field specular microscope primarily for endothelial cell visualization and photography. The optical sectioning possibilities for the microscope were also explored.

II. Scanning Mirror Microscope

Figure 3 is a schematic optical diagram of the system. Illuminated slit *S1* is imaged on the endothelial surface through half of objective *L3*. The illuminated region of the specimen is reimaged through the other half of objective *L3* to a second slit *S2*. The function of slit *S2* is to pass only light that has come from the illuminated slit area in the specimen.

Mirror *M1* oscillates about an axis normal to the diagram. The excursion is about ±2°, giving a total scan of 8° in the reflected beam. The illuminated slit image is thereby scanned in a direction perpendicular to the axis of objective *L3*. However, the slit image formed by the rays returning from the specimen is stationary at slit *S2* because of the second reflection from the oscillating mirror. Lens *L2* serves to collimate the light from slit *S1* for an infinity corrected objective *L3*. Lens *L4* brings the parallel bundle from the objective to a focus at slit *S2*. For an objective with finite tube length correction, different lenses *L2* and *L4* can be selected.

The light that is passed by slit *S2* reflects from the mirror directly behind the slit and then propagates to the third facet of the oscillating mirror. Lens *L5* is a field lens selected to image the second facet of mirror *M1* onto the third facet of *M1*.

After the third reflection from the oscillating mirror the light passes through lens *L6*, which forms an image of slit *S2* in the final image plane *F*. The image of *S2* is scanned across plane *F* by the oscillating mirror. This action essentially lays down the final image, strip by strip.

The mirror oscillates at 500 Hz, so that the image appears continuous to the eye or the camera. With this system the field of view is limited, not by the width of the slit but by the angular field of view of the optics. In particular the microscope objective is typically limited to ~7° full field.

The system can be refined by using a relay system between oscillating mirror *M1* and objective *L3*. The purpose is to image the apex of the mirror onto the aperture plane of the objective, so that as the mirror oscillates there is a minimum of vignetting.

Scanning mirror *M1* is a 1-cm cube with four faces polished and high reflection coated. It is mounted on a resonant torsion rod that is magnetically driven.[10] The amplitude of the oscillation angle is adjustable. The scanning velocity is sinusoidal with time, which leads to a nonuniformity of image illuminance. In practice, however, only the turnaround at the end of the scan produces a change in illuminance that is noticeable photographically. The scan amplitude is normally adjusted so that the turnaround is just outside the field. Then the increase in illuminance toward the end of the scan partially compensates for the normal vignetting of the optical system and yields a satisfactorily uniform field.

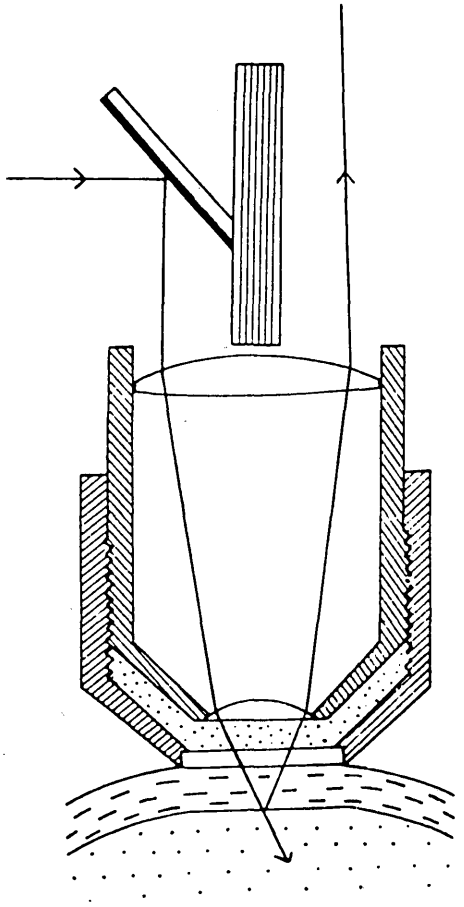

Fig. 2. Divided aperture objective as used by Maurice.[2]

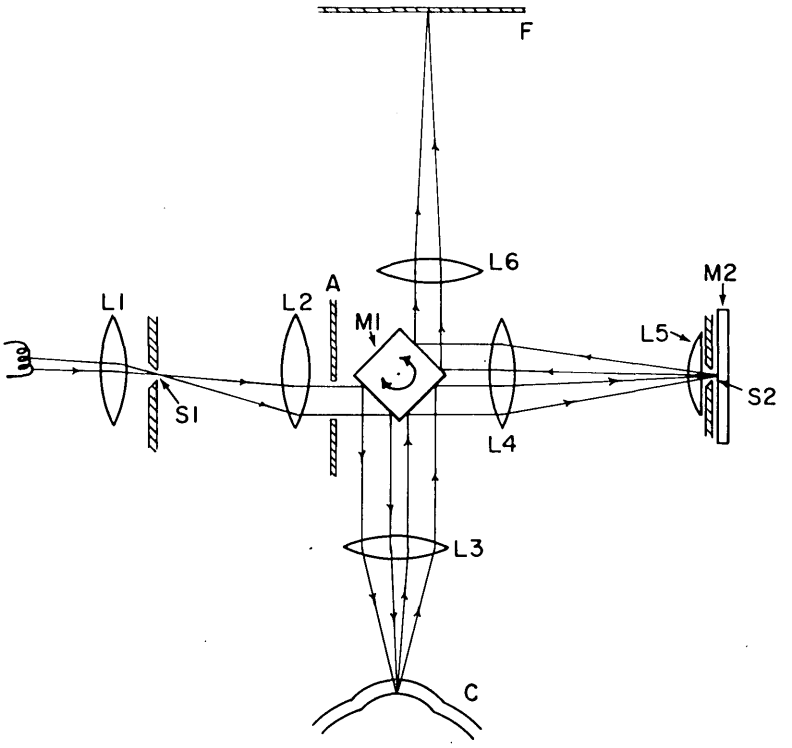

Fig. 3. Schematic diagram of scanning mirror microscope: *L1*, condenser; *S1*, first slit; *L2*, collimator; *A*, rectangular aperture; *M1*, oscillating mirror; *L3*, microscope objective; *C*, cornea; *L4*, telescope lens having the same focal length as *L2*; *L5*, field lens; *S2*, second slit; *M2*, stationary mirror; *L6*, image-forming lens; *F*, film plane or eyepiece image plane.

The arrangement of slit *S2*, mirror *M2*, and field lens *L5* can be modified. For example, a concave mirror of appropriate radius can be used to perform the functions of mirror *M2* and field lens *L5*. This mirror can be masked to form slit *S2*.

III. Optical Sectioning

In Fig. 4, S is the image of the illuminated slit. S is also conjugate to slit *S2* (see Fig. 3). Illumination rays fill the region between the downward-pointing arrows. Image-forming rays occupy the region between the upward-pointing double arrows. Any scattering centers or reflecting surfaces lying within the overlap (crosshatched) region can contribute stray light to the image. Conversely, any scattering or reflecting materials lying outside the crosshatched region such as at plane A cannot cause illumination light to be redirected and superimposed on the image-forming rays. When the scanning mirror is employed, the illuminated region scans back and forth in the x direction, creating an optical section within the specimen.

The thickness of the optical section can be determined directly from the geometry as shown in Fig. 4. Angle θ_n is the minimum angle in the illumination ray bundle, and w is the width of the illuminated slit image. Total thickness $2h$ of the optical section is given by

$$2h = w/\tan\theta_n. \quad (1)$$

The effective optical section thickness is often less than that calculated by Eq. (1). If one considers plane

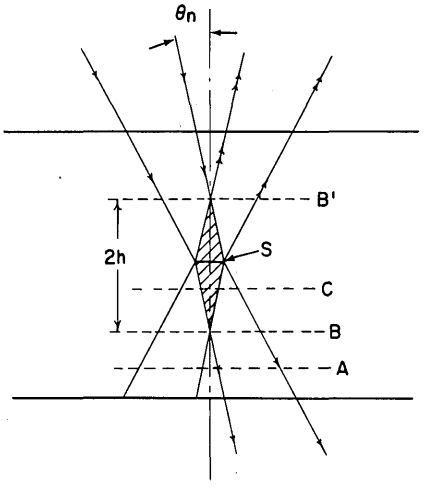

Fig. 4. Ray diagram illustrating optical sectioning characteristics: θ_n, angle of the illumination ray with the minimum inclination; S, image of slit *S1* (the width of the slit image at S is w); $2h$, thickness of the optical section; A, a plane outside the optical section; B' and B, planes at the boundary of the optical section; C, a plane within the optical section. Downward-pointing arrows indicate illumination rays; upward-pointing double arrows indicate image-forming rays. The rays shown are at the edges of the illumination and image-forming bundles. The crosshatched area indicates the region of the specimen in which any light scattered in the direction of the imaging aperture can pass through slit *S2* and reach the image.

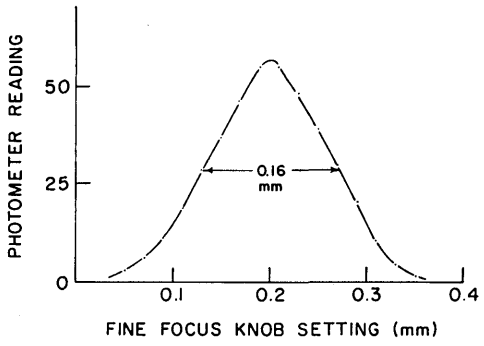

Fig. 5. Image illuminance as a function of focus. 20× objective, water immersed to a specularly reflecting surface, no central aperture stop.

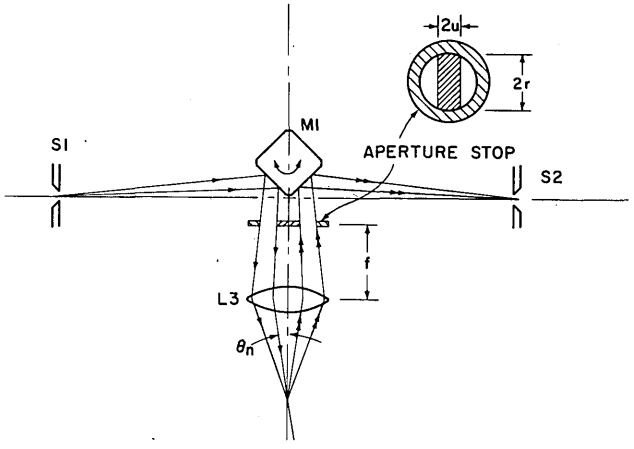

Fig. 6. Partial diagram of scanning mirror microscope with opaque central aperture stop. Symbols are the same as in Fig. 3.

C, the illumination light bundle and imaging ray bundle overlap only partially, so that scattering material in this plane will not contribute as much light to the image as will similar material at the focal plane. The experimentally determined change in illuminance, for a case in which $\theta_n \approx 0$, is shown in Fig. 5.

An effective method for establishing a minimum angle θ_n is illustrated in Fig. 6. At the rear focal plane of objective *L3* an opaque central aperture stop is placed. It has the form of a strip of width $2u$, as illustrated. The minimum angle θ_n is then given by

$$u/r = \gamma_n/\gamma_x = (n \sin\theta_n)/\gamma_x, \tag{2}$$

where γ_x is the N.A. of objective *L3*, n is the index of refraction of the object, r is the radius of the aperture of the objective, and γ_n is defined as $\gamma_n = n \sin\theta_n$. Selection of the optimum value for u is discussed in Sec. V.

An important application of the optical sectioning principle is the elimination of the strong reflection from the anterior surface of the cornea. The reflection coefficient for the air–cornea interface at normal incidence is 0.025. The cornea–aqueous interface (the endothelial cell layer) has a reflection coefficient of 0.00022, 2 orders of magnitude less. Liquid contact to the cornea using an immersion objective is a widely used technique. However, for situations in which it is desired not to touch the cornea, the optical sectioning principle can be used to exclude the reflection from the air–cornea interface as illustrated in Fig. 7. Assuming that the endothelial cell layer is the plane of interest, the requirement is simply that

$$h < t, \tag{3}$$

where t is the thickness of the cornea, and h is the half-thickness of the optical section given by Eq. (1).

Because the exact thickness of the cornea cannot be predicted in advance, it is generally best to select a value of h somewhat less than the nominal value of t, say $h = 0.7t$. Since both w and θ_n in Eq. (1) are under the control of the designer, a given value of h can be obtained over a range of values of either parameter. Optimizing the selection is discussed in Sec. V.

IV. Results

A photomicrograph obtained with the Nikon 20× dipping cone objective is shown in Fig. 8. The dimensions of this particular field are 0.95 × 0.6 mm. This

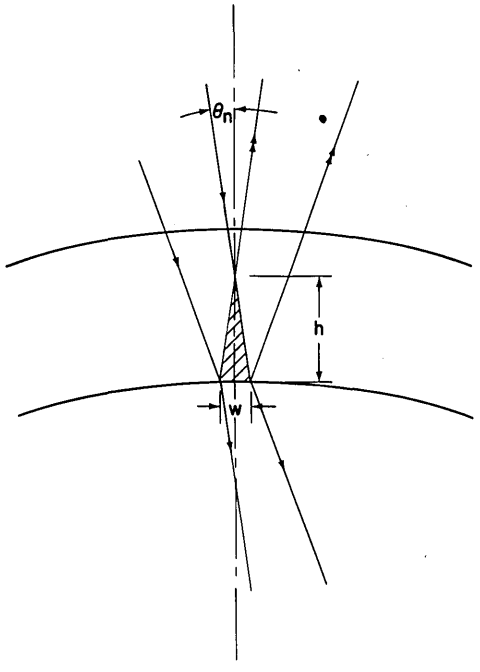

Fig. 7. Optical sectioning effect in the case of noncontact endothelial microscopy. Optical section half-thickness h is made less than the thickness of the cornea so that the air/tear layer surface is outside the optical section.

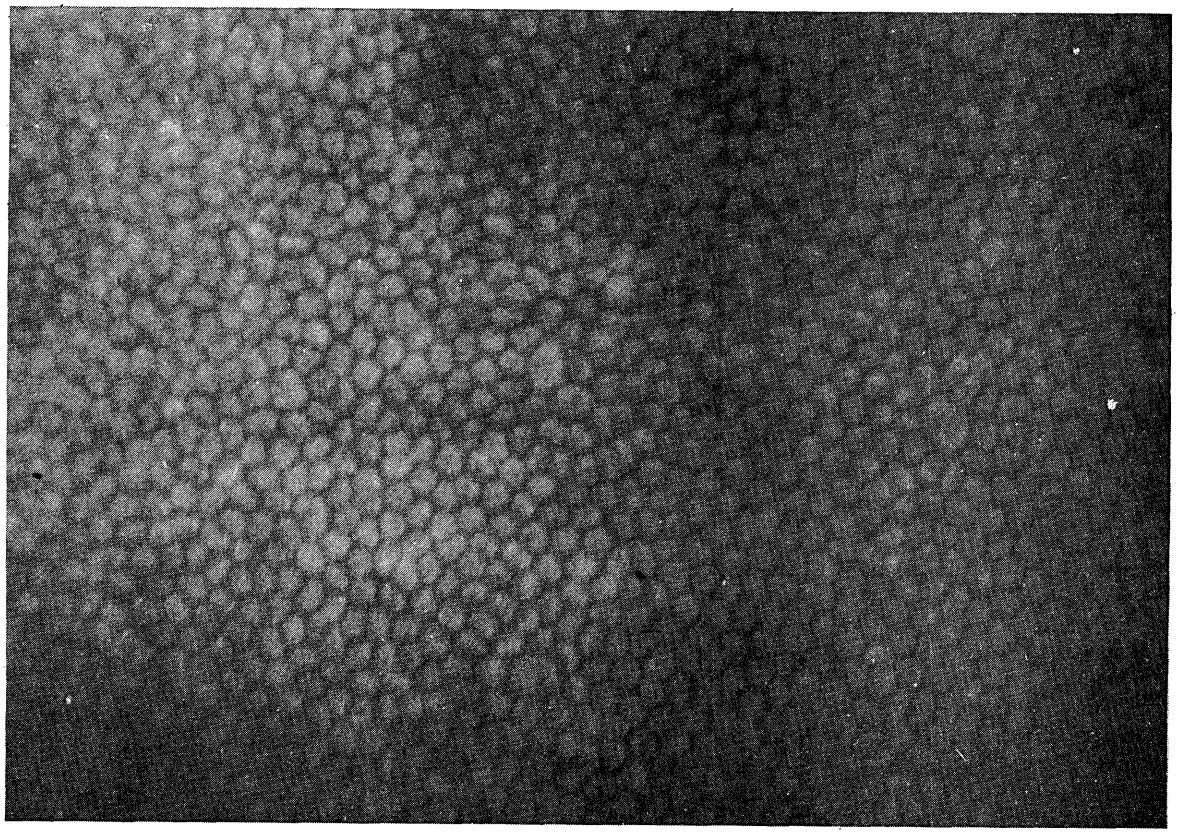

Fig. 8. Rabbit endothelium photographed with the scanning mirror microscope using a 20× Nikon dipping cone objective. Slit width of ~60 μm at the specimen; slit direction horizontal; scan direction vertical. The image dimensions are ~950 × 600 μm, an area of 0.57 mm².

represents a fourteen times increase in area compared with the 0.4 × 0.1-mm image in a conventional specular microscope, an example of which is shown in Fig. 9. Furthermore, the image from the scanning mirror microscope is more uniform in contrast. The conventional image suffers loss of contrast at one side of the slit image, since more illuminated scattering volume overlies that portion of the image. In Fig. 7, this would correspond to the left side of the slit image. In the scanning mirror system any such residual stray light is spread uniformly over the image, making interpretation of images somewhat easier. Furthermore, the slit in the scanning mirror microscope can be narrower than that usually employed in specular microscopes, thus decreasing the quantity of stray light.

The optical sectioning capability is illustrated in Fig. 10. The serial photomicrographs were taken with a 40× water immersion objective.

For noncontact applications a 20× N.A. 0.32 objective with a 6.9-mm working distance was used. The value

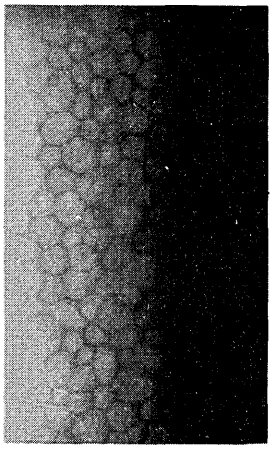

Fig. 9. Endothelial image obtained with a conventional specular microscope. Size of field of cells is ~130 × 370 μm.

of h was selected to be 0.25 mm, ~0.7 times the thickness of the rabbit cornea, which is nominally 0.35 mm. An opaque central stop of width $2u$ = 2.8 mm gave a minimum angle θ_n of 5.6°. Slit image width w = 0.048 mm.

Figure 11 illustrates the images obtained with the noncontact arrangement. As the instrument is aligned relative to the eye, the first image seen is generally that of the anterior surface of the cornea, as in Fig. 11(a). This image aids in centering the system with respect to the apex of the cornea. As the microscope is focused toward the posterior, the strong reflection from the anterior surface disappears, and the endothelial cell layer appears as in Fig. 11(b).

It is obvious that a noncontact instrument has substantial advantages of convenience and freedom from cross-contamination and/or trauma over one that requires contact with the cornea, particularly in a clinical setting. There are trade offs, however, so that each case must be considered according to the results desired. The principal advantage of contact compared to noncontact is related to the frequent involuntary saccadic motion of the eye. With the contact objective placed in contact with the cornea, the lateral motion of the cornea is somewhat damped, and the longitudinal motion of the endothelium relative to the objective is essentially reduced to zero. Neither of these beneficial effects is operating in the case of the noncontact objective. An additional advantage of the contact instrument is that is establishes a fluid interface between the objective and the cornea. It is apparent from Fig. 11(a) that the cornea is not necessarily an optically perfect surface, and therefore the image of the endothelium is likely to be somewhat more aberrated with the noncontact than it is with the contact objective.

Fortunately, the change from contact to noncontact

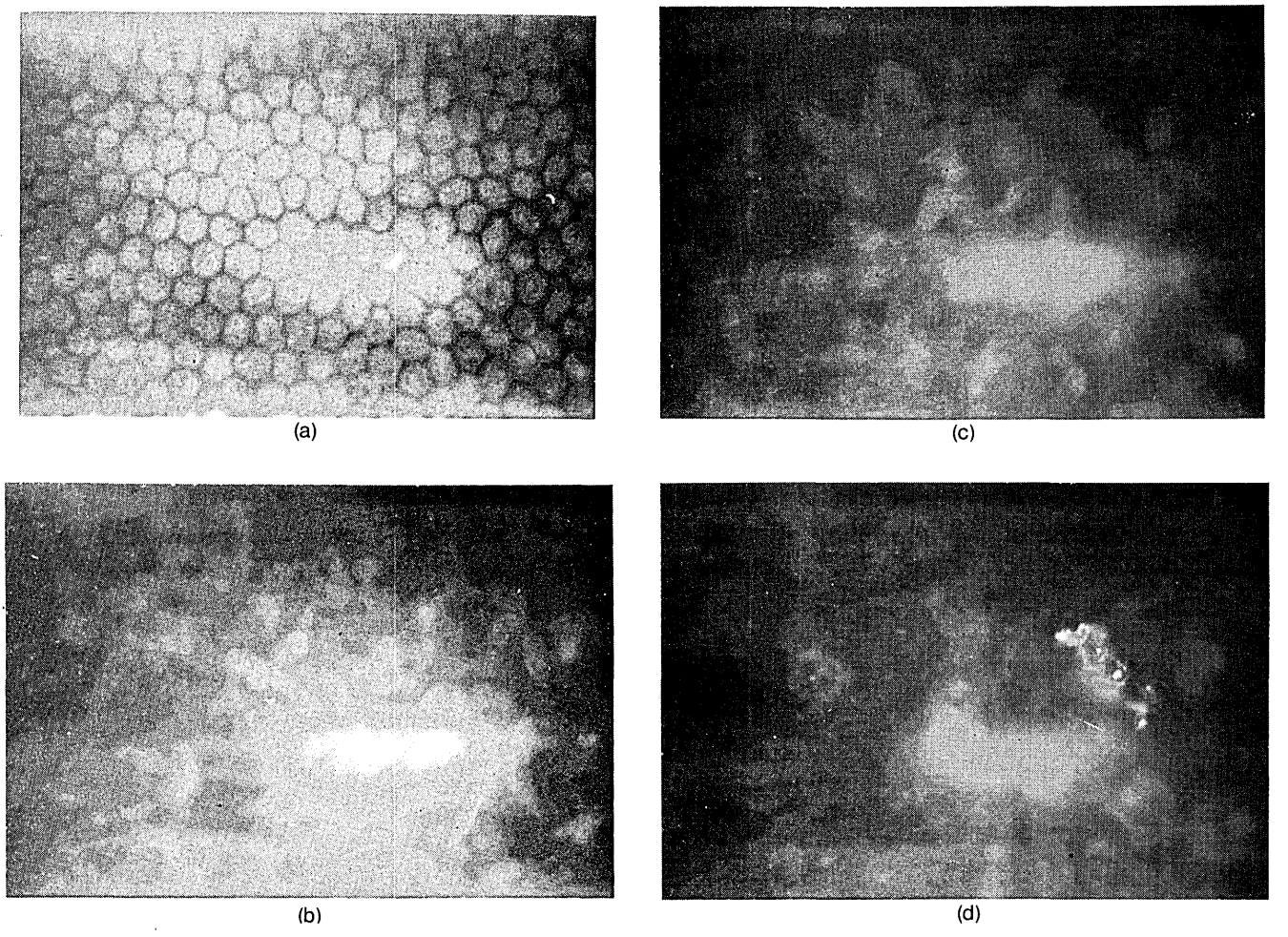

Fig. 10. Serial photomicrographs of a rabbit cornea taken with a 40× N.A. 0.75 objective. A reflection artifact is seen in all four images. (a) microscope focused on the endothelial layer; (b) microscope focused 25 μm anterior to the endothelium using the graduated fine focus adjustment; (c) 100 μm anterior to the endothelium; (d) 370 μm anterior to the endothelium. The cells seen in d are epithelial cells. Field size is ~350 × 280 μm.

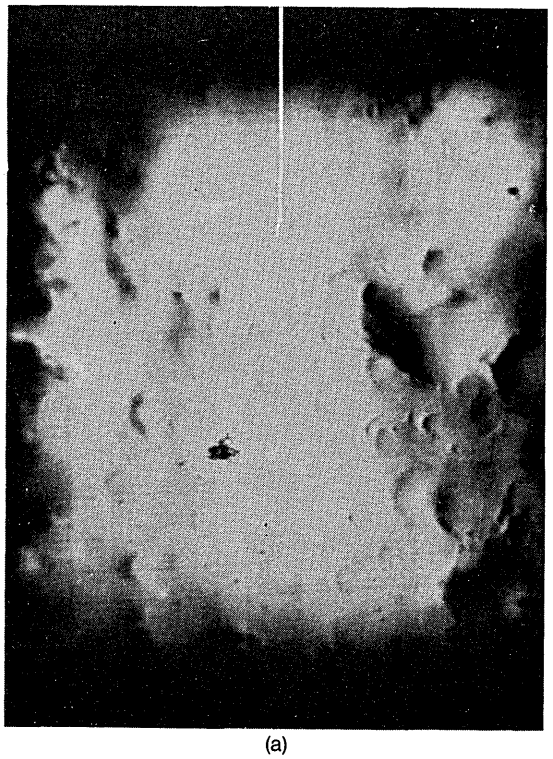

(a)

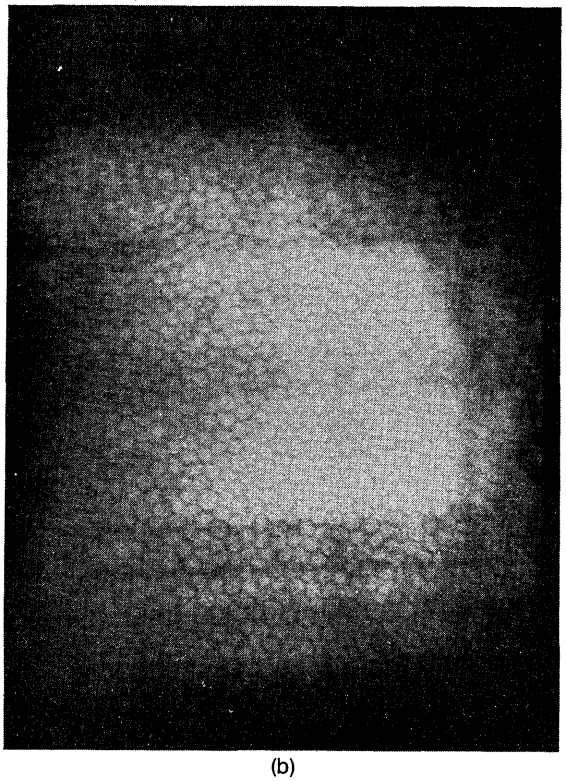

(b)

Fig. 11. Noncontact images of a rabbit cornea: (a) air/tear layer surface with 1/125-sec exposure on ASA 800 film; (b) endothelial cell layer with 0.5-sec exposure on same film. Total field size is ~760 × 1000 μm.

can be as simple as changing objectives, where the noncontact objective has a built-in central stop of the appropriate width.

V. Optimization

As mentioned in Sec. III, a given optical section thickness $2h$ can be achieved in principle by any values of θ_n and w that satisfy Eq. (1). The choice affects light level in the image, field width over which specular reflection occurs, and, to a certain extent, image quality. Depending on the application, it may be desired to optimize for one or another of these parameters.

Considering first the light level, the image illuminance can be optimized as follows. It is assumed that (1) the area of the objective aperture used for illumination is equal to that used for imaging, as illustrated in Fig. 6 and (2) the illuminance provided by the source is uniform at the aperture plane of the objective and is independent of the objective used.

The objective aperture is in the form of the segment of a circle, the area of which is given by

$$A = r^2 \cos^{-1}(u/r) - u^2 \tan \cos^{-1}(u/r), \tag{4}$$

where u is the halfwidth of the opaque central strip, and r is the radius of the objective aperture (Fig. 6).

The quantity $\gamma_n = n \sin\theta_n$, while having the form of the usual numerical aperture, is really an expression of the minimum numerical aperture in one meridian, the plane of the diagram in Fig. 4. It is related to the values of u and r by Eq. (2). Using Eq. (2), Eq. (4) becomes

$$A = r^2 \cos^{-1}(\gamma_n/\gamma_x) - (\gamma_n/\gamma_x)^2 \tan \cos^{-1}(\gamma_n/\gamma_x). \tag{5}$$

Two cases are considered: a specimen that is seen by specular reflection and a specimen that is seen by diffuse reflection. When specular reflection is the principal mechanism for generating image illuminance, the latter is proportional to the area of the objective aperture used for illumination. It is assumed that the imaging aperture is adequate to accept all the specularly reflected light. The image illuminance is also proportional to width w_s of slit *S1*. Therefore,

$$I_s = w_s A, \tag{6}$$

where I_s is a quantity proportional to image illuminance. Width w_s of slit *S1* is related to thickness $2h$ of the optical section, and the minimum angle θ_n through Eq. (1), together with the relation

$$w_s = Mw, \tag{7}$$

where M is the magnification of the system between the slit image at the specimen and slit *S1*.

As illustrated in Fig. 12, illuminance I_s is not monotonic with γ_n. *As* γ_n decreases, A increases, w_s decreases, and the product goes through a maximum. The optimum γ_n for maximum image illuminance is seen to be somewhat less than half the objective N.A.

The second case to be considered is that of diffuse reflection by the specimen. Examples in the case of the eye would be scattering centers within the cornea or within the lens. In this case image illuminance will be

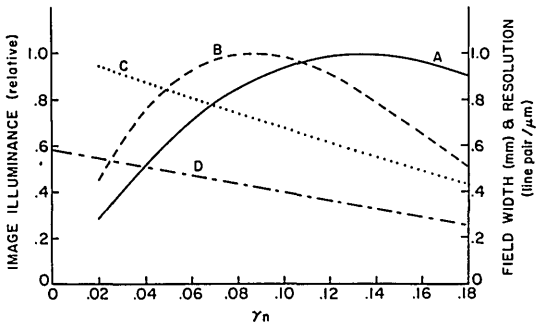

Fig. 12. Image illuminance (relative), field width, and resolution as a function of minimum N.A. γ_n. Calculations are for an objective with N.A. = 0.32. *A*, image illuminance for objective with specular reflection characteristics (calculation is for the center of the field); *B*, image illuminance for object with diffuse reflection characteristics; *C*, field width for a spherical surface with 7.8-mm radius (the cornea); *D*, resolution in lp/μm for lines perpendicular to the scan direction.

proportional to the area of the illumination aperture times the area of the imaging aperture. When these two apertures are equal, as in Fig. 6, the image illuminance is proportional to

$$I_d = w_s A^2, \tag{8}$$

where w_s and A are given by Eqs. (7) and (5), respectively. Figure 12 illustrates the dependence of I_d on γ_n. The optimum value for γ_n is somewhat less than for the case of specular reflection I_s. It should be noted that the optimum value of γ_n does not depend on parameters h, M, or r but only on γ_x and n.

Before selecting the value of γ_n, two other factors need to be considered: image quality and field size. Image quality depends on the minimum N.A. γ_n as well as on the objective N.A. γ_x. The Abbe theory indicates that, for coherent illumination centered in the open aperture, i.e., at $\gamma = \frac{1}{2}(\gamma_n + \gamma_x)$, the minimum resolvable spacing will be $\Delta x = \lambda/\frac{1}{2}(\gamma_x - \gamma_n)$. Because the illumination in the present case is incoherent and fills the aperture from γ_n to γ_x, the minimum resolvable spacing is approximately half of that for the coherent illumination or $\Delta x = \lambda/(\gamma_x - \gamma_n)$. The resolving power defined as Δx^{-1} is shown in Fig. 12.

For curved surfaces such as the cornea, specular reflection is obtained only in a field of limited width, since the rays specularly reflected from sufficiently inclined regions of the surface will not be accepted by the objective. This field is narrower for large values of γ_n than it is for small values, because the range of angles in the illumination and imaging bundles is reduced in the case of large γ_n. In Fig. 12 the dotted line illustrates the width of the field as a function of γ_n. A point of comparison is the normal field size for the objective: 0.90 mm.

The choice of γ_n may depend on the conditions of use. Maximum image illuminance may be desired in some circumstances. In other cases when light level is not the limitation, a smaller γ_n may be selected so as to increase resolution and field size. Since to satisfy Eq. (1) the slit width must decrease as γ_n is decreased, practical problems of slit alignment and freedom from dust become more important as γ_n is reduced.

VI. Discussion

Can the optical section thickness $2h$ be reduced to the point where it is comparable to the depth of field of the microscope? The usual expression for depth of field is[11]

$$d' = \frac{\lambda[n^2 - (\text{N.A.})^2]^{1/2}}{(\text{N.A.})^2},$$

where n is the index of refraction of the specimen, and λ is the wavelength. Since the aperture is not circular in this case, the depth of field can be expected to be different for spatial frequencies with orientations parallel and perpendicular to the scan direction. However, using the depth of field for the full aperture as a limiting case and combining this with the expression for optical section thickness [Eq. (1)], we have

$$w = \frac{\lambda(n^2 - \gamma_x^2)^{1/2}}{\gamma_x^2} \tan \sin^{-1}\left(\frac{\gamma_n}{n}\right). \tag{9}$$

For $\lambda = 0.55$ μm, $\gamma_x = 0.32$, $\gamma_n = 0.135$, and $n = 1.376$, we have $w = 0.95$ μm. While this narrow slit image is possible, the practical problems with very narrow slits become significant. The advantage of such a system is that it could be used to produce photomicrographs of essentially infinite depth of field by translating the specimen (or the microscope) along the axis of the system as the photographic exposure is made.

Applications to specimens other than the cornea are beginning to be explored. A long working distance objective permits interior regions of the human lens to be examined. With an excised mildly cataractous lens, regions of scattering have been photographed at several depths without problems of scattered light from other depths. In general, any transparent or moderately scattering specimen that transmits well enough for transmitted light microscopy can be examined with the scanning mirror microscope by incident light microscopy. Certain opaque materials with rough surfaces can be examined with better contrast using the scanning mirror microscope than using the conventional incident light microscope because regions that are significantly out of focus are not illuminated and therefore do not contribute stray light to the image.

The principle can be extended to a transmitted light system. One method would be to use synchronized scanning mirrors in the illumination and imaging systems. Such a microscope would achieve an optical sectioning effect while retaining the advantages of transmitted light microscopy: bright field of view and contrast generated by the absorbing properties of the specimen.

The skilled craftsmanship and design suggestions of Heinz Rosskothen are much appreciated. The encouragement of this work by Anthony Donn, Charles J. Campbell, Frank B. Hoefle, Calvin W. Roberts, Lawrence G. Pape, and others at the Edward S. Harkness Eye Institute is gratefully acknowledged. This work was supported by the Knights Templar Eye Foundation, Incorporated, and Research to Prevent Blindness, Incorporated.

The material in this paper was presented in part at the annual meetings of the Optical Society of America in November 1978 and October 1979.

References

1. A. Vogt, Graefes Arch. Ophthalmol. **101,** 123 (1920).
2. D. Maurice, Experientia **24,** 1094 (1968).
3. R. A. Laing, M. M. Sandstrom, and H. M. Leibowitz, Arch. Ophthalmol. **93,** 143 (1975).
4. W. M. Bourne and H. E. Kaufman, Am. J. Ophthalmol. **81,** 319 (1976).
5. W. M. Bourne, B. E. McCarey, and H. E. Kaufman, Trans. Am. Acad. Ophthalmol. Otolaryngol. **81,** OP-743 (1976).
6. D. Maurice, Invest. Ophthalmol. **13,** 1033 (1974).
7. S. C. Baer, U.S. Patent 3,547,512 (1970).
8. P. Davidovits and M. D. Egger, Appl. Opt. **10,** 1615 (1971).
9. M. Petran, M. Hadravsky, M. D. Egger, and R. Galambos, J. Opt. Soc. Am. **58,** 661 (1968).
10. Electronics Division, Bulova Watch Co., Inc., Woodside, N.Y. 11377.
11. A. C. Hardy and F. H. Perrin, *The Principles of Optics* (McGraw-Hill, New York, 1932), pp. 510–513.

Meetings Calendar

1980
June

2–4 **Hologram Interferometry and Speckle Metrology, OSA Topical Mtg.,** N. Falmouth, Mass. *OSA, 1816 Jefferson Pl. N.W., Washington, D.C. 20036*

2–4 5th Int. Ultrasonic Imaging and Tissue Characterization Symp., Gaithersburg *M. Linzer, Mater. Bldg. A-366, NBS, Wash., D.C. 20234*

2–6 USNC/URSI/Canadian National Committee URSI, Quebec *J. A. Cummins, Université Laval, Dept de Genie Electriguie, Faculté des Sciences, Cité Universitaire, Quebec G1K7P4*

2–6 6th Int. Conf. on Vacuum Ultraviolet Radiation Physics, Charlottesville, Va. *R. C. Elton, Code 5504, U.S. Naval Res. Lab., Washington, D.C. 20375*

2–6 Gas Diagnostics Course, U. Tenn. *J. W. Bernard, U. Tenn. Space Inst., Tullahoma, Tenn. 37388*

2–6 Quality Control For Photographic Processing, Rochester *College of Graphic Arts and Photography, Rochester Inst. of Tech., One Lomb Dr., Rochester, N.Y. 14623*

2–6 Principles of Color Technology course, Troy *Office of Continuing Studies, Rensselaer Polytechnic Inst., Troy, N.Y. 12181*

4–6 2nd Int. Ultrasonic Materials Characterization Symp., Gaithersburg *H. Berger, Physics Bldg. B-312, NBS, Wash., D.C. 20234*

5–6 3rd World Chromatography Conf., Zurich *V. M. Bhatnagar, Alena Enterprises of Canada, P.O. Box 1779, Cornwall, Ont.*

9 Radiometry Using Silicon Photodiodes workshop, NBS Gaithersburg *J. L. Tech, Radiometric Physics Div., NBS, Washington, D.C. 20234*

9–11 Fiber Optic and Electro-Optic System Design course, Wash., D.C. *Cont. Ed. Program, George Wash. U., Wash., D.C. 20052*

9–13 Principles of Color Technology course, Troy *Office of Continuing Studies, Rensselaer Polytechnic Inst., Troy, N.Y. 12181*

9–13 Fundamentals of Electro-Optical Systems Analysis course, UCLA *Cont. Ed. Engr., Math., UCLA Ext., P.O. Box 24902, Los Angeles, Calif. 90024*

9–13 Modern Optics for Scientists and Engineers Course, Vail *Laser Inst. Am., P.O. Box 9000, Waco, Tex. 76710*

10 Ann. CORM Tech. Conf., Gaithersburg *F. W. Billmeyer, Jr., Dept. Chem., Rensselaer Polytechnic Inst., Troy, N.Y. 12181*

16–17 Optical Design Using Desktop Computers Course, Rochester *Sinclair Optics, 20 N. Main St., Pittsford, N.Y. 14534*

16–17 Color Technology For Management course, Troy *Office of Continuing Studies, Rensselaer Polytechnic Inst., Troy, N.Y. 12181*

16–20 Holography And Optical Processing, Gordon Res. Conf. *A. Cruickshank, Gordon Res. Conf., Colby-Sawyer Coll., New London, N.H. 03257*

16–20 Infrared Technology: Fundamentals and Systems Applications Course, U. Mich. *Eng. Summer Confs., 400 Chrysler Ctr., N. Campus, U. Mich., Ann Arbor, Mich. 48109*

16–20 Microscopy for Pharmaceutical Scientists Course, Chicago *N. Daerr, McCrone Res. Inst., 2508 S. Michigan Ave., Chicago, Ill. 60616*

16–20 High Power Lasers Course, Vail *Laser Inst. Am., P.O. Box 9000, Waco, Tex. 76710*

18–20 AAS Meeting, College Pk., Md. *L. W. Frederick, P.O. Box 3818, Univ. Station, Charlottesville, Va. 22903*

18–20 **Picosecond Phenomena, OSA Topical Mtg.,** N. Falmouth, Mass. *OSA, 1816 Jefferson Pl. N.W., Washington, D.C. 20036*

21–25 Int. Lens Design Conf., U. Calif., Santa Cruz *OSA, 1816 Jefferson Pl. N.W., Washington, D.C. 20036*

continued on page 1793